Predictive Current Control of the Three-Level Four-Leg Active Filter Based on In-Phase Carrier Modulation

Li Delu[1](✉), Fang En[2], Liu Zhijian[1], and Zhang Kailiang[2]

[1] Jiangsu Vocational Institute of Architectural Technology, Xuzhou, China
[2] Jiangsu Province Key Laboratory of Intelligent Industry Control Technology, Xuzhou University of Technology, Xuzhou, China

Abstract. To reduce the complex calculation of three-level spatial vector modulation (SVPWM) in practical applications, improve the compensation performance of active filters (AF), and combine with the same-phase carrier modulation strategy, a predictive current control strategy based on the same-phase carrier is proposed. The strategy outputs a small voltage harmonic component and reduces the computational complexity of the modulation strategy. The effectiveness of the modulation strategy proposed in this paper is verified by simulation experiments.

Keywords: Electric electronics · In-phase carrier modulation · Predictive current

1 Introduction

Multilevel converter technology reduces voltage stress in the main power device and has less harmonic content in the output voltage by using a mature low-voltage device stacking combination to become a high-voltage converter [1–4]. Because of these characteristics, three-level AF are widely used [3, 5–9].

Three-level four-leg (TF) is one of the common active filter structures, and its modulation strategy has been widely concerned. Common modulation methods include phase-shifted carrier PWM method (PS-PWM), voltage space vector modulation (SVPWM) method, and phase disposition PWM method (PD-PWM).

Because the phase-shifted carrier PWM method has the same reference voltage and carrier frequency, the output energy and switching losses distribution of each unit is more even, which is beneficial to device selection and thermal design. Because of its simple realization and the advantages of power balance between units, it has been widely used in industry [8, 10, 11]. SVPWM strategy needs to be located in a specific triangle in voltage vector space before selecting spatial vector synthesis. This method has many voltage redundancy vectors, complex calculation and selection, and does not take into account the power balance distribution between the units when selecting spatial vectors. phase disposition PWM method has a better harmonic output effect than carrier shift phase modulation, but its carrier is distributed vertically, resulting in uneven power between units, which makes it rarely used in practice [5].

© ICST Institute for Computer Sciences, Social Informatics and Telecommunications Engineering 2022
Published by Springer Nature Switzerland AG 2022. All Rights Reserved
D. Jiang and H. Song (Eds.): SIMUtools 2021, LNICST 424, pp. 342–358, 2022.
https://doi.org/10.1007/978-3-030-97124-3_26

There are eight switch tubes in the TF active filter, which makes the carrier and modulation wave of three-level modulation technology more than two levels, more than one. And each carrier and modulation wave have multiple degrees of control, including frequencies, modulation amplitude values, modulation waves and carrier offsets. The different combinations of degrees of freedom have produced a variety of carrier PWM technology and based on the in-phase carrier modulation technology developed at two levels, a in-phase carrier prediction current control strategy for TF AF is proposed. The strategy is easy to implement, has a clear physical meaning, greatly reduces computing time, and better adapts to the rapid response requirements of harmonic compensation.

2 Carrier Modulation Strategy for Three-Level Four-Leg Active Filter

2.1 Basic Principles of Three-Level Four-Leg Active Filter

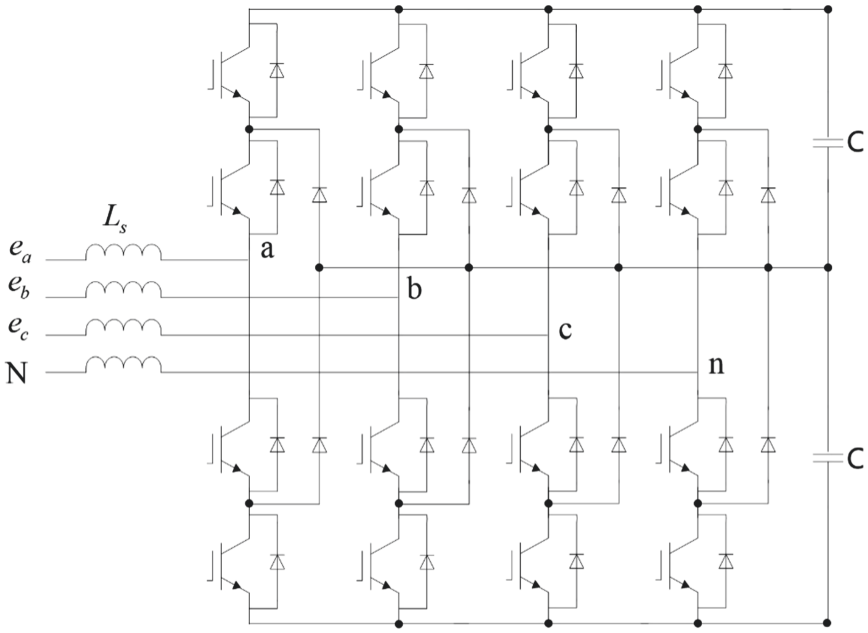

Fig. 1. Three levels Four-leg topology

In the above figure, the midline connecting inductor is selected to be consistent with the three-phase connecting inductor, and L_s is the connecting inductor, where the internal resistance of the inductor is ignored. i_{sa}, i_{sb}, i_{sc}, i_{sn} represent grid-side current. i_{la}, i_{lb}, i_{lc}, i_{ln} represent nonlinear load current (including midline current), which can be decomposed into fundamental component i i_{fa}, i_{fb}, i_{fc}, i_{fn} and harmonic component i_{ha}, i_{hb}, i_{hc}, i_{hn}, $i_{la} = i_{fa} + i_{ha} i_{lb} = i_{fb} + i_{hb} i_{lc} = i_{fc} + i_{hc} i_{ln} = i_{fn} + i_{hn}$. The compensation current generated by APF is expressed as i_{ca}, i_{cb}, i_{cc} and i_{cn}. The PWM inverter is controlled to make the following:

$$\begin{cases} i_{ca} = -i_{ha} \\ i_{cb} = -i_{hb} \\ i_{cc} = -i_{hc} \\ i_{cn} = -i_{hn} \end{cases} \tag{1}$$

So

$$\begin{cases} i_{sa} = i_{la} + i_{ca} = i_{fa} \\ i_{sb} = i_{lb} + i_{cb} = i_{fb} \\ i_{sc} = i_{lc} + i_{cc} = i_{fc} \\ i_{sn} = i_{ln} + i_{cn} = i_{fn} \end{cases} \tag{2}$$

The above is the basic principle of parallel APF.

2.2 Carrier Lamination PWM Method

Carrier Lamination PWM control technology is directly developed from the two-level SPWM, usually, for N-level carrier modulation, the need for (N-1) amplitude and frequency of the same triangular carrier, two sets of carriers distributed in the positive and negative half-week, divided into two layers of upper and lower cascades, modulation of the same modulation wave, so the name.

According to the phase relationship between carriers, the control method of the three-level midpoint clamp-type inverter can be divided into in-phase carrier PWM control and reversed-phase carrier PWM control, that is, with a pair of amplitude and frequency equivalent triangular carriers stacked up and down, distributed in the modulation wave of the positive and negative half wave. When the modulation wave is larger than the upper triangular carrier on the positive half axis, the output is high, when the modulation wave is smaller than the lower triangular carrier on the negative half axis, and when the modulation wave is between two triangular carriers, the output level is 0. In sine modulation waves, for example, Fig. 2 shows reversed-phase carrier PWM control, and Fig. 3 shows in-phase carrier PWM control.

Reversed-Phase Carrier PWM Control

Taking the three-phase single-phase bridge arm as an example, the reversed-phase carrier PWM control principle as shown in Fig. 2, U_A for the sine modulation wave of the A-phase bridge arm, U_P and U_N for the triangular carrier distributed in its upper and lower half waves.

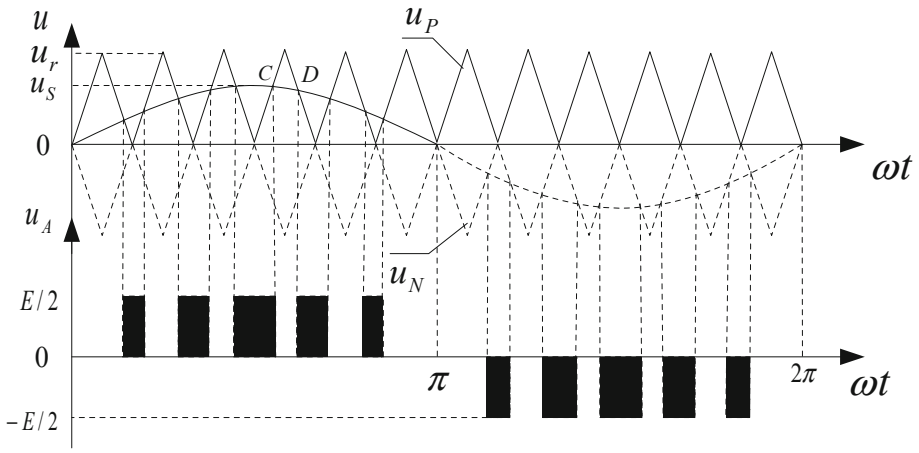

Fig. 2. Reversed-phase carrier PWM control

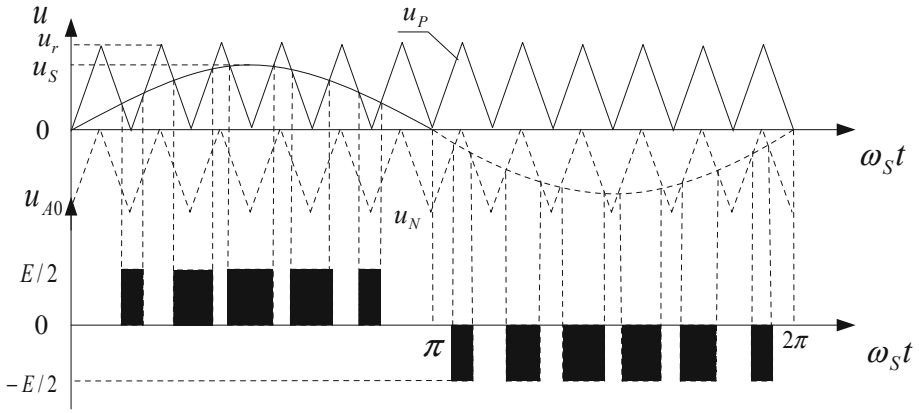

Fig. 3. In-phase carrier PWM control

The modulation wave U_A is compared with the triangular carrier U_P and U_N, respectively. In the positive half wave, $|U_A| \geq |U_P|$, the positive PWM pulse is triggered, so that the upper arm is turned on and the output level is 1. In the negative half wave, $|U_A| \leq |U_N|$, the negative PWM pulse is triggered to make the lower bridge arm turn on and output level -1. In a modulation wave period, the carrier is oddly symmetric about π.

$$U_P = \begin{cases} -(\omega_c t + \theta - 2k\pi)\frac{U}{\pi} + U, \ \ 2k\pi - \theta \leq \omega_c t \leq 2k\pi + \pi - \theta \\ (\omega_c t + \theta - 2k\pi)\frac{U}{\pi} + U, \ \ 2k\pi + \pi - \theta \leq \omega_c t \leq 2k\pi + \pi - \theta \end{cases} \tag{3}$$

Where U is the amplitude of the carrier, θ is the initial phase angle of the triangular carrier, and ω_c is the angular frequency of the carrier.

The equation for modulation waves is:

$$u_A = U_S sin\,\omega_s t$$

Where U_S is the amplitude of the modulation wave, and ω_s is the angular frequency of the modulation wave.

As shown in Fig. 2 the modulation wave intersects the carrier at sampling point C, D, and at sampling point C:

$$U_S sin\,\omega_s t = -(\omega_c t + \theta - 2k\pi)\frac{U_r}{\pi} + U_r \tag{4}$$

The following can be found:

$$\omega_c t = 2k\pi + \pi - \theta - \pi M\ sin\,\omega_s t \tag{5}$$

At sampling point D there is:

$$\omega_c t = 2k\pi + \pi - \theta + \pi M\ sin\,\omega_s t \tag{6}$$

Where $M = U_S/U_r$ is the modulation.

When $w_c t \in [2k\pi + \theta, 2k\pi + \pi + \theta]$, you get a time function for the output of the three-level single-bridge arm SPWM:

$$U_{AO} = \begin{cases} 0\ \omega_c t \begin{cases} < 2k\pi + \pi - \theta - \pi M sin\omega_s t \\ \geq 2k\pi + \pi - \theta + \pi M sin\omega_s t \end{cases} \\ \frac{E}{2}\ \omega_c t \begin{cases} < 2k\pi + \pi - \theta + \pi M sin\omega_s t \\ \geq 2k\pi + \pi - \theta - \pi M sin\omega_s t \end{cases} \end{cases} \tag{7}$$

E is the DC side voltage value.

Analysis of the formula (7) with Fourier stages gives the following formula:

$$U_{AO}(\omega_c t, \omega_s t) = \frac{1}{4}MEsin\omega_s t + \frac{E}{2m\pi}\sum_{n=1,2,\cdots}^{\infty}\sum_{n=\pm1,\pm3,\cdots}^{\pm\infty} e^{-jma}J_n(mM\pi)sin[(mF+n)\omega_s t] \tag{8}$$

The above shows that the DC component is zero in the voltage of the carrier inverted PWM control output, and the amplitude of the base wave component is 1/4ME.

In-Phase Carrier PWM Control

In-phase carrier PWM control principle as shown in Fig. 3, two sets of triangular carriers U_P and U_N phases are the same, its carrier waveform is asymmetrical to the x-axis, The same as reversed-phase carrier PWM control, the modulation wave U_A is compared with the triangular carrier U_P and U_N, respectively. In the positive half wave, $|U_A| \geq |U_P|$, the positive PWM pulse is triggered, so that the upper arm is turned on and the output level is 1. In the negative half wave, $|U_A| \leq |U_N|$, the negative PWM pulse is triggered to make the lower bridge arm turn on and output level −1. The difference is to write out two carrier expressions:

$$U_P = \begin{cases} (\omega_c t - 2k\pi)\frac{U_r}{\pi}, 2k\pi \leq \omega_c t \leq 2k\pi + \pi \\ -(\omega_c t - 2k\pi)\frac{U_r}{\pi} + 2U_r, 2k\pi + \pi \leq \omega_c t \leq 2k\pi + 2\pi \end{cases} \tag{9}$$

$$U_{s1} = \begin{cases} U_S \sin \omega_s t, 0 \le \omega_s t \le \pi \\ 0, \pi \le \omega_s t \le 2\pi \end{cases} \tag{10}$$

$$U_N = \begin{cases} (\omega_c t - 2k\pi)\frac{U_r}{\pi} - U_C, 2k\pi \le \omega_c t \le 2k\pi + \pi \\ -(\omega_c t - 2k\pi)\frac{U_r}{\pi} + U_r, 2k\pi + \pi \le \omega_c t \le 2k\pi + 2\pi \end{cases} \tag{11}$$

$$U_{s2} = \begin{cases} U_S \sin \omega_s t, \pi \le \omega_s t \le 2\pi \\ 0, 0 \le \omega_s t \le \pi \end{cases} \tag{12}$$

Where U_r for the amplitude of the carrier, ω_c for the angular frequency of the carrier, U_S for the amplitude of the modulation wave, ω_s for the angular frequency of the modulation wave.

Referring to the method of retrieving the reversed-phase PWM control expression, From the expression of in-phase carrier PWM control method, phase voltage output U_{AO1} and U_{AO2} can be obtained, then analyzed by Series of Fourier, and the output formula is:

$$U_{AO}(\omega_c t, \omega_s t) = \frac{1}{4} MEsin\omega_s t \pm \frac{2E}{m\pi^2} \sum_{m=1,3,\cdots}^{\infty} \sum_{v}^{\infty} \frac{1}{2l-1} J_{2l-1}(mM\pi) cosmF\omega_s t \pm$$
$$\frac{2E}{m\pi} \sum_{m=2,4,\cdots}^{\infty} \sum_{n=\pm 1,\pm 3,\cdots}^{\pm\infty} J_n(mn\pi) \sin[mn\pi] sin[(mF+n)\omega_s t] \tag{13}$$

The above shows that in the voltage of the carrier's phase PWM control output, the DC component is zero, the base wave component amplitude is 1/4ME, the presence of m is even, n is an odd carrier up and down frequency harmonics, and the carrier and the odd carrier harmonics are included.

Simulation Comparison Under MATLAB/Simulink

In MATLAB/Simulink environment, the carrier phase PWM control and carrier inverter PWM control were simulated and compared, and the carrier ratio was set to 40, and the sine modulated wave line voltage amplitude was 380V and the frequency was 50 Hz.

Figure 4 is the line voltage U_{AB} waveform output by reversed-phase carrier PWM control, and Fig. 5 is the line voltage U_{AB} waveform output by in-phase carrier PWM control.

From Fig. 6 and Fig. 7, the line voltage output during in-phase carrier control contains less harmonic content than reversed-phase carrier control. After double Fourier analysis and simulation comparison, it can be concluded that: the output phase voltage of the two carrier lamination PWM methods does not contain a constant component. In the phase voltage of the carrier phase control method output, the harmonic energy is mainly concentrated in the carrier frequency, and the other harmonics are mainly integer multiple carrier frequency as the center of the edge band harmonics, the magnitude is smaller. In the phase voltage output of the reversed-phase carrier control method, there is an edge band harmonic centered on the integer carrier frequency, with a larger magnitude. At the same time, the line voltage waveform effect of the in-phase carrier PWM control output of the same phase stack is better than that of the reversed-phase carrier PWM control, and this paper will use the in-phase carrier PWM control to control the TF active filter.

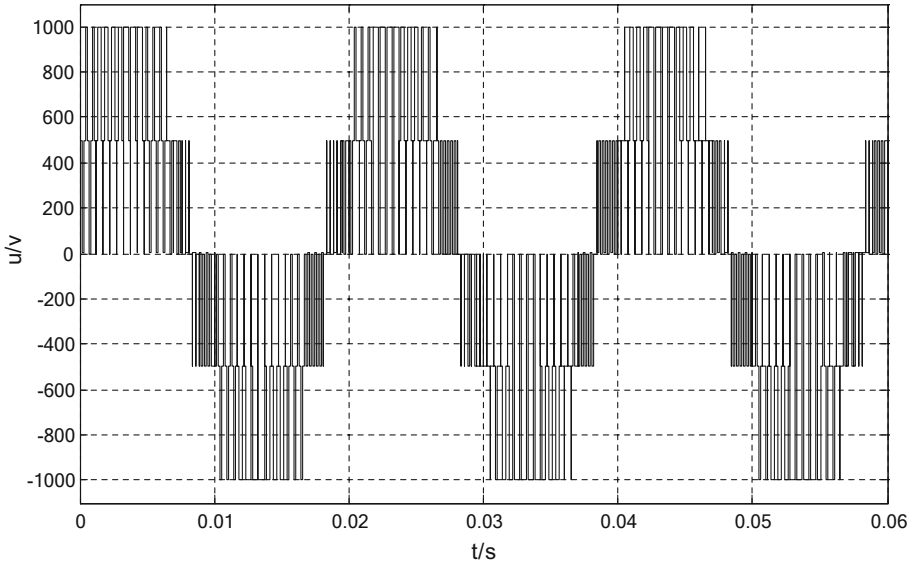

Fig. 4. Reversed-phase carrier PWM method controls the output line voltage.

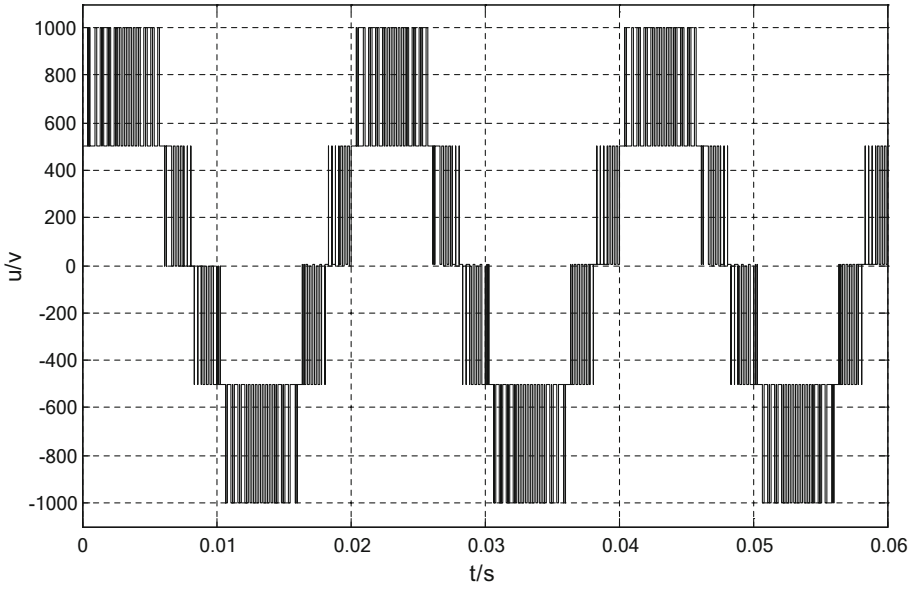

Fig. 5. The in-phase carrier PWM method controls the output line voltage.

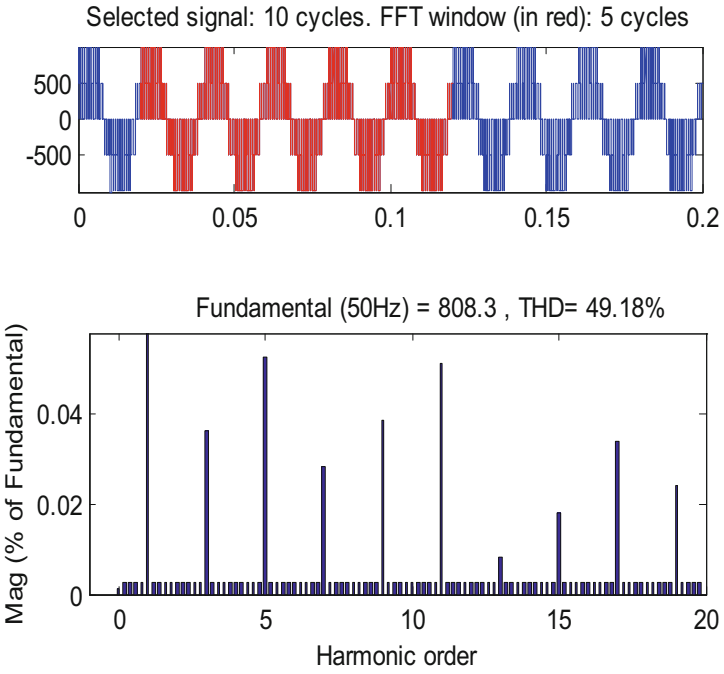

Fig. 6. FFT analysis of the inverted carrier control output line voltage (Color figure online)

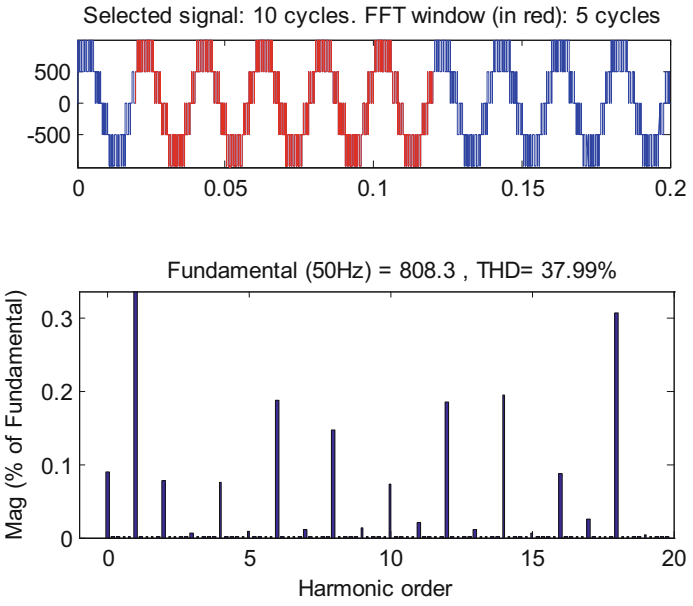

Fig. 7. FFT analysis of the output line voltage with phase carrier control (Color figure online)

3 Harmonic Current Prediction Control

Predictive current control mainly uses the state information of the current sampling time to calculate the command current value of the next sampling time and the APF reference output voltage prediction value, to predict the trajectory of the next sampling cycle to compensate for the current and determine the switching pulse of each switching device of the TF APF, so that the output current of the active filter can accurately and quickly track the change of the command current [12–15].

As can be seen from the topology of the active filter for the four-leg in Fig. 1.

$$\begin{cases} L_S \frac{di_{Fa}}{dt} = -R_s i_{Fa} + e_a - u_{aN} \\ L_S \frac{di_{Fb}}{dt} = -R_s i_{Fb} + e_b - u_{bN} \\ L_S \frac{di_{Fc}}{dt} = -R_s i_{Fc} + e_c - u_{cN} \\ L_S \frac{di_{Fn}}{dt} = -R_s i_{Fn} - u_{nN} \end{cases} \tag{14}$$

In order to obtain the APF AC side output voltage prediction value at the next sampling time, the discretization of the upper stage is approximated to:

$$\begin{cases} u^*_{aN}(k+1) = -\frac{L_S}{T_S}\left[i^*_{Fa}(k+1) - i_{Fa}(k)\right] - R_s i_{Fa}(k) + e_a(k) \\ u^*_{bN}(k+1) = -\frac{L_S}{T_S}\left[i^*_{Fb}(k+1) - i_{Fb}(k)\right] - R_s i_{Fb}(k) + e_b(k) \\ u^*_{cN}(k+1) = -\frac{L_S}{T_S}\left[i^*_{Fc}(k+1) - i_{Fc}(k)\right] - R_s i_{Fc}(k) + e_c(k) \\ u^*_{nN}(k+1) = -\frac{L_S}{T_S}\left[i^*_{Fn}(k+1) - i_{Fn}(k)\right] - R_s i_{Fn}(k) \end{cases} \tag{15}$$

Where $u^*_{xN}(k+1)$(x takes a, b, c, n) represents the three-phase output voltage prediction value of the k1 sampling time compensator, $i^*_{Fx}(k+1)$(x takes a, b, c, n) is the current prediction value of the k1 sampling time instruction and is the sampling cycle of the T_s compensator system.

The principle of the current predictive control strategy is as follows. Firstly, whether the harmonic current generated by the load is a steady state is determined. The steady state means that the harmonic instruction current presents periodic changes. The data at the corresponding time of the previous system cycle can be used to replace the compensation current instruction value $i^*_{Fx}(k+1)$ at k + 1. If the harmonic current generated by the load is transient, it indicates that the compensation current instruction value $i^*_{Fx}(k+1)$ at time k + 1 does not have periodicity, and it needs to be calculated by the second-order extrapolation interpolation method.

The error limit is set ε here, when $\left|i^*_{Fx}(k) - i^*_{Fx}(k-N)\right| < \varepsilon$, the harmonic current generated by the load is determined to be steady, at this time the last cycle command current storage value can be obtained from the compensation device under the use of the instruction current value at the moment, that is:

$$i^*_{Fx}(k+1) = i^*_{Fx}(k-N+1) \tag{16}$$

Where N is the number of sampling points for an industrial frequency cycle, when the compensator system samples at 10 kHz. $N = 0.02 \times 10^4 = 200$.

When $\left|i_{Fx}^*(k) - i_{Fx}^*(k-N)\right| \geq \varepsilon$ established, the harmonic current generated by the load is determined to be transient, at which time the load current changes greatly, and the instruction current value of the next sampling time of the compensator is predicted by using the Lagrange interpolation method, i.e.:

$$i_{Fx}^*(k+1) = 3i_{Fx}^*(k) - 3i_{Fx}^*(k-1) + i_{Fx}^*(k-2) \tag{17}$$

According to the above command current prediction method, we can quickly get the command current prediction value of the TF APF at the next sampling moment, it can be $i_{Fx}^*(k+1)$. Replaced it by Eq. (15) to obtain the next sampling moment APF AC side output voltage reference value $u_{xN}^*(k+1)$, and finally use the same phase stack sine PWM modulation algorithm to produce a turn-off pulse of the TF APF power switch device, so as to accurately and quickly track the change of command current, to achieve the purpose of rapid compensation harmonics.

4 Predictive Control Simulation Based on Same-Phase Carrier Modulation

4.1 Simulation Model

The principle of predictive control has been discussed separately in the previous section, where a simulation model of TF AF using voltage-free sensor $p - q - r$ harmonic detection, predictive current control, and phase carrier modulation is established. The system simulation diagram is as follows (Fig. 8):

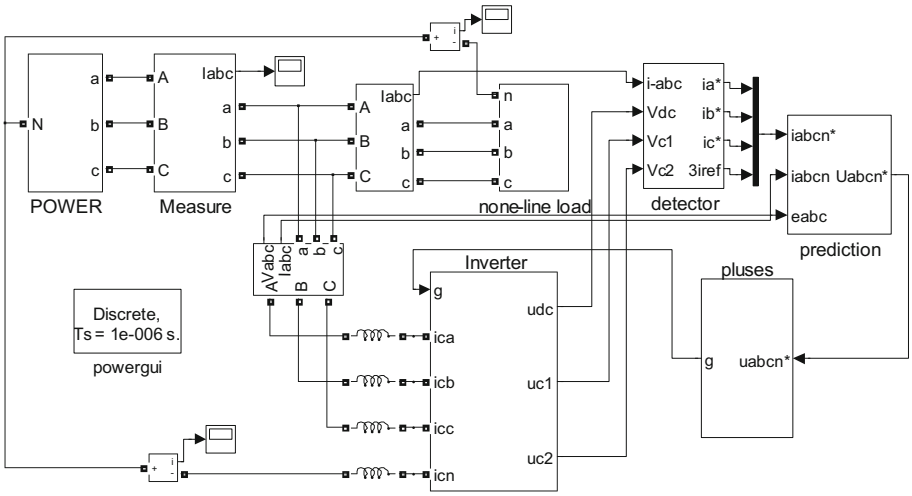

Fig. 8. A system simulation diagram predicting current control.

The simulation system consists of a power supply module, a nonlinear load module, a harmonic detection module, a predictive current control module and a TF with phase carrier module. The carrier module is shown in Fig. 9, and the main power tube switch states of the three levels of power level are represented by the bridge arm output, respectively, in the figures of 1100, 0110, and 0011.

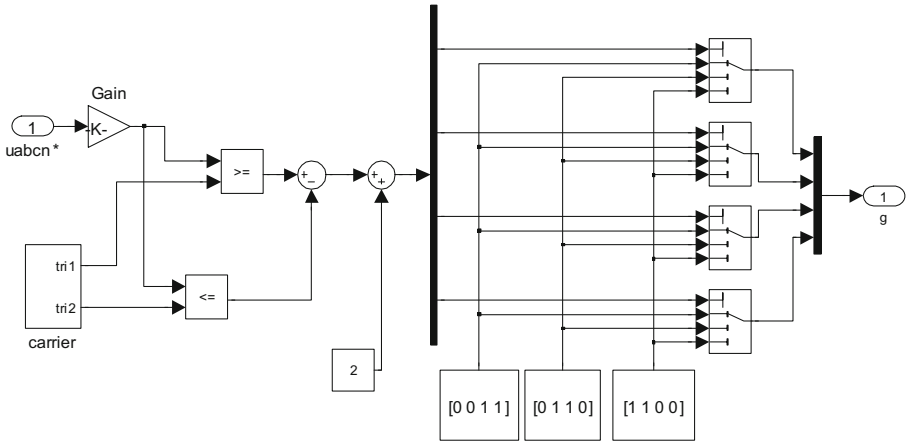

Fig. 9. Three-level four-leg carrier modulation module

The simulation conditions are as follows: grid voltage 380 V, 50 Hz, the nonlinear load is three-phase non-controlled rectifier bridge and A-phase single-phase non-controlled rectifier bridge, APF access point network inductive value is 1mH, DC side voltage is 1000 V, system sampling frequency 10 kHz, and compensation scheme is real-time compensation harmonics.

4.2 Simulation Results

Figure 10 shows the induction current and the predicted command current obtained by the advance link calculated by the p-q-r detection method, and it can be seen that the predicted instruction exceeds the previous switching cycle, but the calculation error of the current inflection point is large; Fig. 11 is the DC side voltage, the lower capacitor voltage and the DC side voltage of the three-level APF.

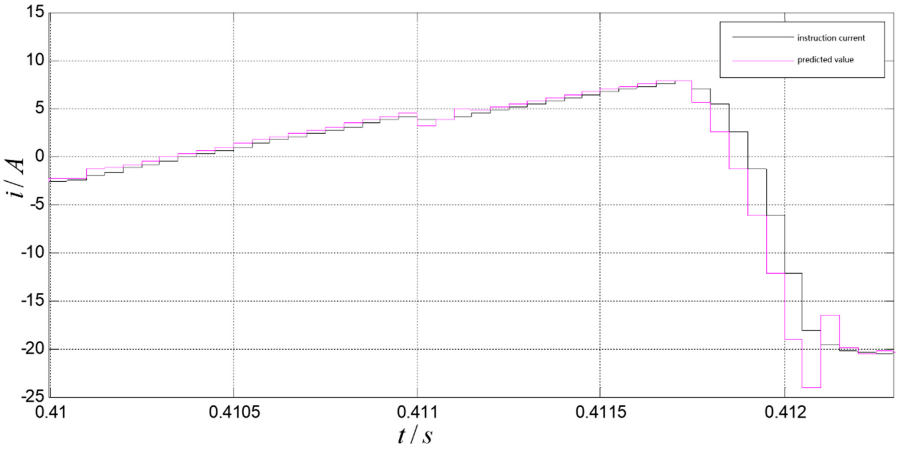

Fig. 10. Instruction current and its predicted value

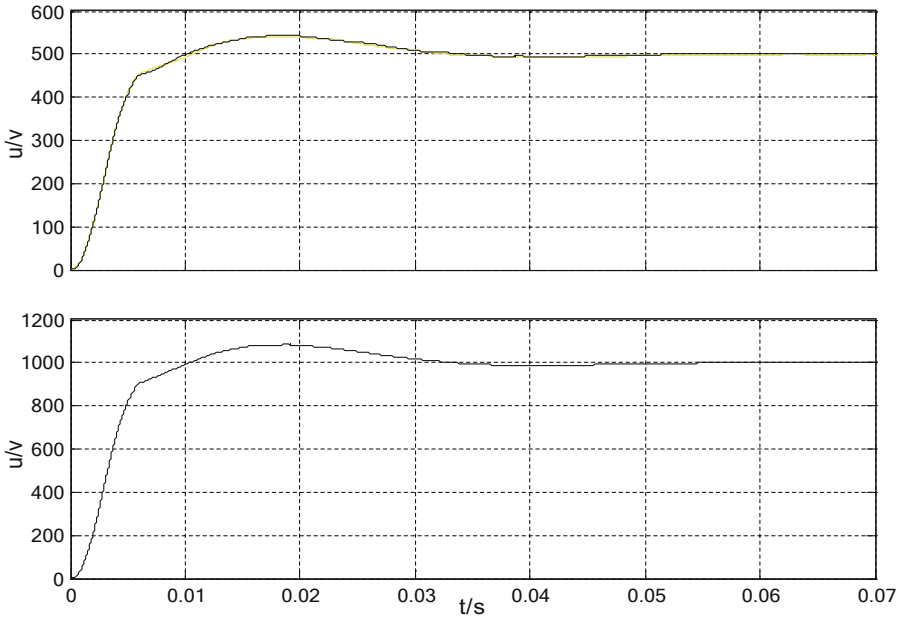

Fig. 11. DC side up and down capacitive voltage and total voltage

Figure 12 is the case where the APF phase output current tracks the phase command current. Figure 13 shows compensate for the current before and after the power supply. As can be seen, the supply current after APF compensation is basically a sine wave. The total harmonic distortion rate (THD) of the supply current was reduced from 18.45% before compensation to 3.76%, and the current harmonic component was effectively suppressed.

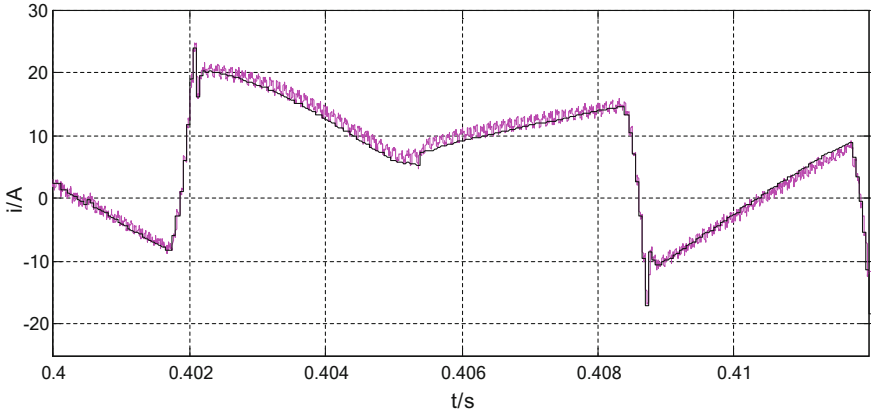

Fig. 12. Phase A command current tracking

Figure 14 is the APF Fourth Leg Output Current Tracking the Midline Command Current. Figure 15 shows compensate for the front and rear midline currents. The magnitude of the midline current before compensation is 20 A, and the magnitude and energy of the medium line current after compensation is greatly reduced.

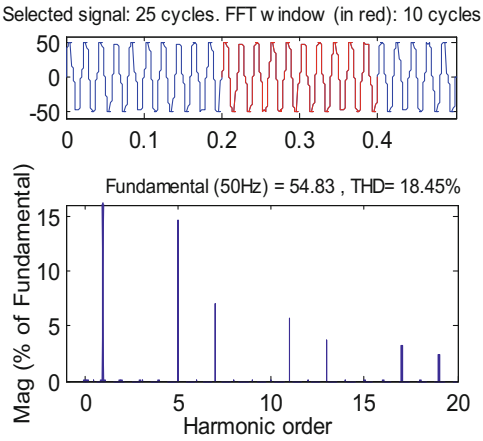

(a) Before the A-phase current is compensated

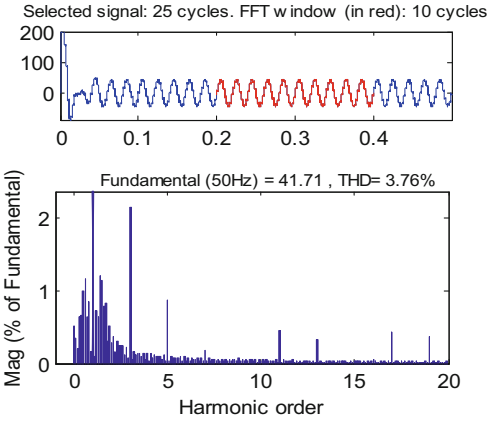

(b) After the A-phase current is compensated

Fig. 13. 1analysis before and after phase a current compensation

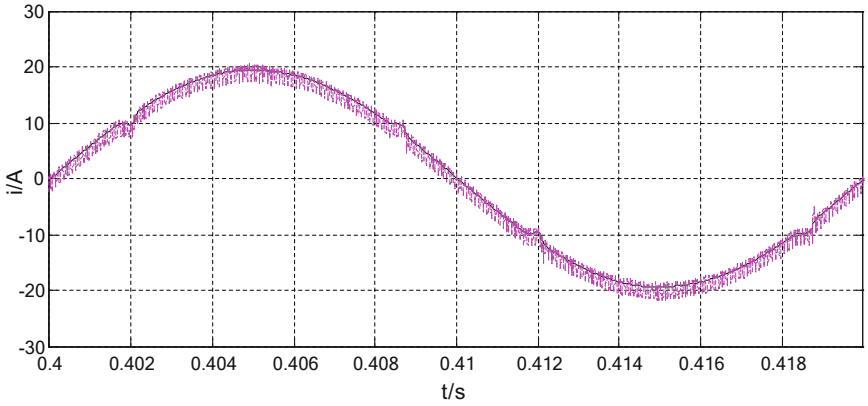

Fig. 14. Midline instruction current tracking

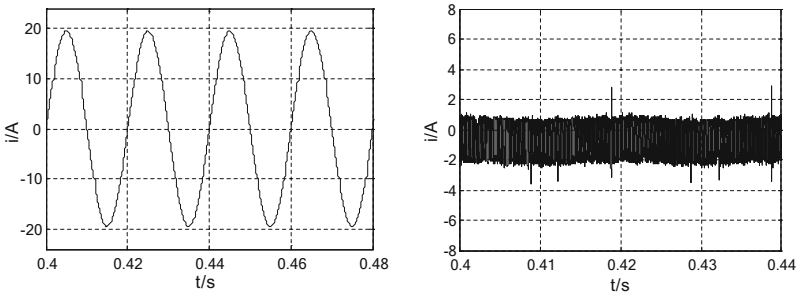

Fig. 15. Front and rear waveforms for current compensation for the midline

5 Conclusion

Through the analysis of carrier lamination PWM method strategy, a predictive current control strategy based on the same phase carrier modulation is proposed. Applying this strategy, the theoretical analysis and simulation of the active filter control system of the four-leg of the three levels are carried out. The simulation results show that:

1) The same-phase carrier modulation strategy output voltage harmonic performance is better. The harmonic component content is smaller.
2) Compared with the SVPWM modulation strategy, based on the predictive current control strategy of the same phase carrier, the physical significance is clear, the calculation time is greatly reduced, and the rapid compensation of harmonics can be realized.

Acknowledgement. The authors acknowledge the Jiangsu University Natural Science Research Project (18KJB470024) and Funding Project for Professional Leaders of Higher Vocational Colleges in Jiangsu Province (2020GRGDYX070). This work was supported by Scientific Research Project of Jiangsu Vocational Institute of Architectural Technology in 2019 (JYA319–13).

References

1. Wang, B.F., Liu, M., Yuan, T.L., Zhang, Z.H.: Study on topological structure of medium voltage active power filter. Dianli Zidonghua Shebei/Electr. Power Autom. Equip. **26**(6) (2006)
2. Waware, M., Agarwal, P.: Performance investigation of multilevel inverter based active power filter in distorted high voltage supply system (2010). https://doi.org/10.1109/ICSET.2010.5684961
3. Madhukar, W., Agarwal, P.: Comparison of control strategies for multilevel inverter based active power filter used in high voltage systems (2010). https://doi.org/10.1109/PEDES.2010.5712440
4. Waware, M., Agarwal, P.: Use of multilevel inverter for elimination of harmonics in high voltage systems. In: 2010 The 2nd International Conference on Computer and Automation Engineering, ICCAE 2010, vol. 2 (2010). https://doi.org/10.1109/ICCAE.2010.5451518
5. Hasim, A.S.B.A., Dardin, S.M.F.S., Ibrahim, Z.B., Azid, A.B.A., Ishak, A.M.B.: Comparative study; different types of PWM control scheme in three-phase four-wire shunt Active Power Filter (APF) topology (2019). https://doi.org/10.1109/ICECOS.2018.8605234
6. Dai, G., Zhao, D., Lin, P., Zhang, C.: Study of control strategy for active power filter based on modular multilevel converter. Dianli Xitong Baohu yu Kongzhi/Power Syst. Prot. Control, **43**(8) (2015)
7. Ziani, A.C., Llor, A.M., Fadel, M.: Geometrical approach of current predictive control for four-leg converters (2011). https://doi.org/10.1109/ISIE.2011.5984430
8. Li, J., Hu, C., Wang, L., Zhang, Z.: APF based on multilevel voltage source cascade converter with carrier phase shifted SPWM. In: IEEE Region 10 Annual International Conference, Proceedings/TENCON, vol. 1 (2003)
9. Geethalakshmi, B., DelhiBabu, K.: An advanced modulation technique for the cascaded multilevel inverter used as a shunt active power filter (2011). https://doi.org/10.1109/IICPE.2011.5728123
10. Li, J.L., Li, J., Wang, L.Q., Zhao, D.L., Zhang, Z.C., Xu, H.H.: Carrier phase shifted SPWM and its applications in shunt APF. Dianli Xitong Zidonghua/Autom. Electric Power Syst. **30**(9) (2006)
11. Sun, Y.Q., Yin, Q., Sheng, J., Pan, W.T.: Variable-frequency carrier bands PWM (VFCB-PWM) and its applications in shunt APF. Dianli Xitong Baohu yu Kongzhi/Power Syst. Prot. Control, **38**(10) (2010)
12. Du, G., Li, J., Liu, Z.: The improved model predictive control based on novel error correction between reference and predicted current. In: Conference Proceedings - IEEE Applied Power Electronics Conference and Exposition - APEC, March 2018. https://doi.org/10.1109/APEC.2018.8341528
13. Yu, J., Teng, Z., Zhang, J., Hu, K.: Predictive current control and stability analysis of active power filter. Diangong Jishu Xuebao/Trans. China Electrotechnical Soc. **24**(7) (2009)

14. Li, G., Zhao, C., Zhou, M., Li, G., Chen, Z.: A predicted control scheme of single phase active power filter in electric traction system. In: IEE Conference Publication, **478** I (2001). https://doi.org/10.1049/cp:20000372
15. Usama, M., Jaehong, K.: Simplified Model Predicted Current Control Method for Speed Control of Non-Silent Permanent Magnet Synchronous Motors (2020). https://doi.org/10.1109/iCoMET48670.2020.9073884